Annual Technical Report

DE-NA0002375

University of Utah

The UQ-Predictive Multidisciplinary Simulation Center for High Efficiency Electric Power Generation with Carbon Capture

Carbon Capture Multidisciplinary Simulation Center

Philip J. Smith, Principal Investigator

Philip.smith@utah.edu   801-585-3129

April 1, 2019 through March 31, 2020

April 30, 2020

Annual Technical Report
DE-Na0002375
April 1, 2019 through March 31, 2020

Carbon Capture Multidisciplinary Simulation Center
University of Utah – Institute for Clean and Secure Energy

The Carbon Capture Multidisciplinary Simulation Center (CCMSC) was established in 2014 by ASC/PSAAP2 to demonstrate positive societal impact of extreme computing by deployment of low-cost, low-carbon energy solution for power generation. The overall strategy has included collaboration with our industrial partners, General Electric Power and Ontario Power Generation, and an inter-disciplinary focus on development of technology. Three teams contribute to the overarching predictive design: the computer science team, the physics team and the validation/ UQ team.

Our final site visit from the ASC/PSAAP team was held on January 27th. Participating reviewers included the following.

> David Etim - Federal Program Manager at NNSA
> Tim Germann - Director of Exascale Co-Design Center for Materials in Extreme Environments (ExMatEx), Los Alamos National Laboratory
> John Feddema –AST—Sandia National Laboratories
> Robert Ferencz – Division Leader, Computational Engineering, Lawrence Livermore National Laboratory
> Antoinette "Tina" Macaluso –AST—Leidos, Inc.,
> Robert "Bob" Voigt –AST—Leidos, Inc.,
> Marianne Francois – Program Manager, Los Alamos National Laboratory
> Eric Phipps – Senior Technical Staff, Sandia National Laboratories
> Erik Draeger – Deputy Director of Application Development, Exascale Computing Project, Lawrence Livermore National Laboratory
> Robert Hoekstra – Technical Manager, Sandia National Laboratories
> Ben Bergen – Research Scientist, Los Alamos National Laboratory

OUTREACH AND EDUCATION
Current Students and Post-doctoral Associates

- Teri Draper, Ph.D. candidate, University of Utah
- Jebin Elias, Ph.D. candidate, University of Utah
- John Holmen, Ph.D. candidate, University of Utah
- Damodar Sahasrabudhe, Ph.D. candidate, University of Utah

- Pavol Klacansky, Ph.D. candidate, University of Utah
- Joshua McConnell, Ph.D. candidate, University of Utah
- William Usher, Ph.D. candidate, University of Utah
- Kamron Brinkerhoff, M.S. candidate, Brigham Young University
- Arun Hegde, Ph.D. candidate, University of California-Berkeley
- Oscar Diaz-Ibarra, post-doctoral research associate, University of Utah
- John Camilo Parra-Alvarez, post-doctoral research associate, University of Utah

Post-degree Employment

- Christopher Earl, staff member, Lawrence Livermore National Laboratory

- Ben Schroeder, staff member, Sandia National Laboratory-Berkeley

- Alexander Abboud, staff member, Idaho National Laboratory

- Aaditya Landge, software engineer, Twitter

- Pascal Grosset, staff member, Los Alamos National Laboratory

- Mark Kim, staff member, Oak Ridge National Laboratory

- Troy Holland, post-doctoral associates, Los Alamos National Laboratory

- Oscar Diaz-Ibarra, post-doctoral research associate, University of Utah

- John Camilo Parra Alvarez, post-doctoral research associate, University of Utah

- Siddharth Kumar, asst. professor, Computer Science, Univ. of Alabama, Birmingham

- Siddartha Ravichandran, staff member, Expedia

- Michael D. Brown, staff, Hi-Rez Studios

- Alex Josephson, post-doctoral fellow, Los Alamos National Laboratory

- Babak Goshayeshi, senior scientific software engineer, Merck & Company

- MinMin Zhou, senior engineer, Reaction Engineering International

- Daniel Gunderson, engineer, Big West Oil Refinery

- Joshua McConnell, post-doctoral research associate, University of Utah

- Kaitlyn Scheib, teacher, School for Independent Learners

- Andrew Richards, post-doctoral fellow, Los Alamos National Laboratory

- Jim Oreluk, post-doctoral fellow, Sandia National Laboratory-Berkeley

- Oscar Diaz-Ibarra, post-doctoral fellow, Sandia National Laboratory-Berkeley

- Alan Humphrey, Sandia National Laboratory

- Benjamin Isaac, Lawrence Livermore National Laboratory

- Aaron Knoll, Intel

Internships and Lab Visits

<u>Kamron Brinkerhoff</u> secured a summer internship at Los Alamos National Laboratory which has been placed on hold due to the pandemic of corona virus.

<u>Oscar Diaz-Ibarra</u> *(post-doctoral research associate)* visited Los Alamos National Lab in November 2019. He was hosted by Duan Zhong Zhang and Susan Kurien. He made multiple research presentations to staff of the lab.

COMPUTER SCIENCE: EXASCALE RUNTIME, VISUALIZATION, I/O, DSL

Lassen porting efforts continued with focus on supporting use of hypre within Arches builds using the Kokkos::CUDA back-end. This work addresses limitations of past work by replacing a custom portable Arches linear solve (demonstrated with the helium plume model at the last review) with use of hypre. This in-progress port of Arches' hypre-based linear solve identified limitations of Uintah's current support for Kokkos::CUDA. Specifically, lack of support for modifiable variables and re-sizing of variables in the GPU data warehouse to support Arches' use of different sized variables across tasks. Work is underway to address these limitations for heterogeneous Kokkos-based Arches runs across both host and device on Lassen. As a part of this work, support for Kokkos::CUDA within problematic tasks exposing the limitations was removed to ease fixes and incremental refactors for correctness, debugging output and test cases were implemented to more easily identify such problematic tasks and infrastructure, and Uintah's Unified Scheduler was extended to support transferring variables from device-to-host for variables existing first on the device and needed for subsequent tasks on the host.

A paper was written using Uintah's adoption of Kokkos to demonstrate an approach for indirectly adopting a performance portability layer in large legacy codes. This accepted paper describes use of a framework-specific portability layer between the application developer and the adopted performance portability layer to help improve legacy code support and long-term portability, shares lessons learned when adopting Kokkos in Uintah through discussion on loop-level, application-level, and build-level details for easing adoption of a portability layer, and demonstrates Kokkos capabilities using this approach with Kokkos::OpenMP and Kokkos::CUDA across multicore-, many-core-, and GPU-based nodes for Arches' char oxidation model and Uintah's reverse Monte-Carlo ray tracing-based radiation model.

The Computer Science team collaborated with the Arches team to simplify existing data accessors. Once simplified in production code, changes were carried into the branch maintaining Uintah's latest Kokkos support with portable implementations added to support portable non-Kokkos, Kokkos::OpenMP and Kokkos::CUDA builds. This work updated accessor calls across ~1,200 variables and 90 files while eliminating seven unnecessary call variants in application code and twenty-four unnecessary implementation variants behind-the-scenes. Continuing hypre work, the Arches team provided a stand-alone problem stressing Arches' use of hypre itself as

well as a simple boiler problem. The former was used to port and validate use of the Arches hypre-based linear solve with Kokkos::OpenMP and Kokkos::CUDA.

Problems provided by the Arches team were used to begin addressing infrastructure limitations identified by earlier work. As a part of this work, modifies support was added to validation of device-side variable copies, modifies support was added to processing of device-side ready variables, and heterogeneous build issues were addressed. Specifically, previously hard-coded bulletproofing specific to use of Kokkos::OpenMP and Kokkos::CUDA individually for various Arches code and synchronization mechanisms was extended to support heterogeneous builds using Kokkos::OpenMP and Kokkos::CUDA simultaneously. Additionally, Uintah was transitioned from SVN to Git and Git-equivalent workflows were identified and documented to help ease the transition. As a part of this work, all prior commit history for the master branch was merged into the branch maintaining Uintah's latest Kokkos support to ease debugging and development moving forward.

The Computer Science team has continued to collaborate closely with the Arches teams to support their adoption of Kokkos within Arches. In addition to the above work, key aspects of this support include (i) providing debugging support, (ii) keeping the branch maintaining Uintah's latest Kokkos support up-to-date with Uintah's production codebase, and (iii) incrementally moving this branch towards being production ready with continued far-reaching updates across Arches for fixes, standardization, and maintainability.

The Visualization Team focused on expanding the coupled simulation-machine layout for in situ performance analysis to include multi-threading metrics. The primary focus was on the visualization of thread metrics at the thread and node level based on the thread assignment. As with other performance metrics, they were custom metrics measured within the Uintah framework and utilized our custom collection class previously developed for other performance metrics.

Additionally, the collection of MPI communication performance metrics was refactored to be finer grained, on a per task basis which allowed for greater interrogation of the tasks that dominate the inter-rank communication. This collection was coupled with a new technique for the displaying multivariate metrics via stacked plots.

Lastly, the custom collection class has now replaced all of the previous ad-hoc collection of performance metrics. As a result, all performance metrics are now centrally accessible for both visualization and log files with standardized output.

PHYSICS

LES Integration

- Supported the Atikiokan production runs with feature additions, bug fixes, and general runtime support.

- Participated in the analysis of two radiometer models based on the Reverse Monte Carlo and Orthogonal sweeps radiation models.

- Developed turbulence analysis tools, including turbulence forcing and enstrophy monitoring for idealized isotropic turbulence scenarios enabling further evaluation of the various turbulence models within Arches and in pursuit of research interests or turbulence particle coupling.

- Participated in a Stokes analysis on the Oxy-Fired Combustor to highlight the particle turbulence interactions. This work was compiled into a paper and is being refined for submission.

- Performed a Bayesian-based analysis of the percent resolved TKE in the target Atikokan boiler to enable simulation quality monitoring. This is an original application of the UQ work in the center applied to LES quality evaluation.

- Participated in a Bayesian-based analysis to obtain verification error estimates on key QOI's for the Atikokan boiler as a function of mesh resolution. This also was a novel application of the center's UQ work.

- Worked tightly with the CS team towards hardware portability for the UCF and Arches. As a result, the CS team adopted some Arches constructs for data warehouse management and the Arches performance portability layer was streamlined with guidance and suggestions from the CS group. A geometrically reduced, but still physics-rich boiler problem was defined together with the CS team as a target for demonstrating Arches/ UCF performance portability.

- Maintained Arches continuously through regression testing, verification testing, and performance evaluations

RMCRT: Virtual radiometer

Our implementation of the RMCRT Virtual Radiometer (VR) was re-factored to only support the Arches component. The VR mimics a physical radiometer instrument and is useful when comparing with experimental data. Originally, the code was developed inside the On-The-Fly data analysis modules which allowed multiple Uintah components to utilize the code. This worked for small scale proof-of-concept simulations but proved to be confusing to users and difficult for developers to maintain and extend. No other components have used the Virtual Radiometer since its creation so we elected to incorporate it directly within the Arches component. This simplified the code by allowing the removal of several layers of interface code.

Significant effort was spent improving the VR so it could be used in production simulations. As mentioned above, the radiometer code was used in scaling studies and in small proof-of-concept simulations. CCMSC developers have repeatedly found that when code is taken into the production environment bugs and over sights are often identified. Effort was spent on the user interface, adding bulletproofing and generalizing the code so any number of radiometers could be specified. Each radiometer can be now be located anywhere in the domain and have unique properties (orientation, solid angle and number of rays).

In conjunction with the VR development the Discrete-Ordinates radiation model implementation was re-factored. Significant effort was spent on:
  - Implementation clean-up, code modernization and enforcement of coding standards.
  - Eliminated redundant code and collapsed code into reusable methods.
  - Removed unused routines and variables.
  - Use of more descriptive and consistent variable naming convention.
  - Eliminated based 1 arrays used in Fortran routines. No more confusing +1, -1 offsets.
  - Improved and added additional bulletproofing.
  - Removed confusing variables that had have multiple definitions.

During this development, we found it necessary to modify our uda comparison tools to insure results were not altered. Users can now include or exclude variables during uda-to-uda comparisons.

The Buildbot is an open-source framework, written in Python, that is used for automated software compilation and regression tests of the Uintah applications. With every commit, four compilation tests (cpu:opt, cpu:debug, cpu:static, gpu) are executed and approximately 350 regression tests are performed to check for software correctness. This framework is being continually improved by adding new features so developers can diagnose failed tests and test software patches before committing them to the common repository. During year 5 additional buildslaves were added to include kokkos:opt, kokkos_opt-omp, kokkos:opt-cuda and kokkos:opt-omp-cuda build compilation tests. To improve extensibility and maintainability of the python scripts, the methods for compiling and running tests were re-factored and generalized. Great care must be exercised whenever this framework is modified since it provides a early warning to developers that there's a problem with their code when a test fails.

Recent changes to the infrastructure forced a complete rewrite of the post processing utility that analyzed individual task timings on a per core basis. During a code optimization cycle, developers would enable the task timings output, run the simulation and on each core a file would be created containing all of the task timings averaged over 10 timesteps. The files also contained MPI communication information. The utility would process all the files, aggregate the data and identify the 10 tasks that took the longest time to complete. This performance data would then guide the developer to the tasks that were candidates for optimization. The number of files that the utility had to processed could be very large, depending on the machine and simulation problem.

During year 5 CCMSC/Uintah developers decided to move from svn to github so effort was spent modifying the buildbot testing suite and nightly regression testing scripts to accept the new revision control system commands.

Development of Instrument Models
As part of the validation/uncertainty quantification (V/UQ) short course taught by Prof. Sean Smith and Prof. Philip J. Smith for CCMSC faculty and staff, we worked on projects to determine L1500 furnace radiative flux and intensity measurement uncertainties using Bayesian methods coupled with instrument models. These projects served as a launching point for the targeted validation experiments (TVEs) and instrument model developments summarized below.

<u>Narrow-angle Radiometer – Radiative Intensity</u> As part of the TVE process, we worked with graduate student Teri Snow to calibrate narrow-angle radiometers multiple times. Each calibration was a refinement of the previous calibration in an effort to reduce the uncertainty in the calibration data. We developed detailed instrument models for the radiometer when it was used in the calibration mode and in actual combustion operation, as these were slightly different. These additional physics reduced the computed Bayesian posterior uncertainty of the model parameters and consequently of the radiation intensity results. We then used these uncertain parameters together with radiometer voltage and temperature measurements to compute the Bayesian posterior predictive, the radiative intensity with uncertainty in the L1500 from the November 2018 campaign.

We used one of the radiometers at Pacificorp's Hunter Power Plant during a coal/biomass cofiring demonstration in August of 2019. We made slight modifications to the instrument model for use at the plant. We collected intensity measurements on the 9th, 10th, 12th, and 14th floors of the boiler during both the coal and coal/biomass tests. An example of the results from the Bayesian analysis is shown in Figure 1. For this analysis, we used the August 2018 (uneven heating) calibration data. A comparison between the intensity results firing the coal and the coal/biomass blend is shown in Figure 2.
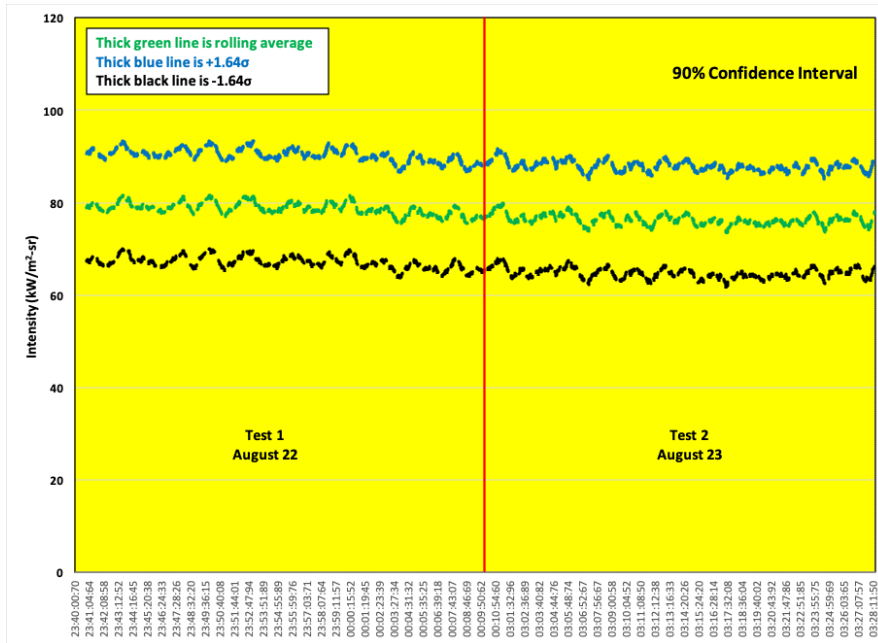
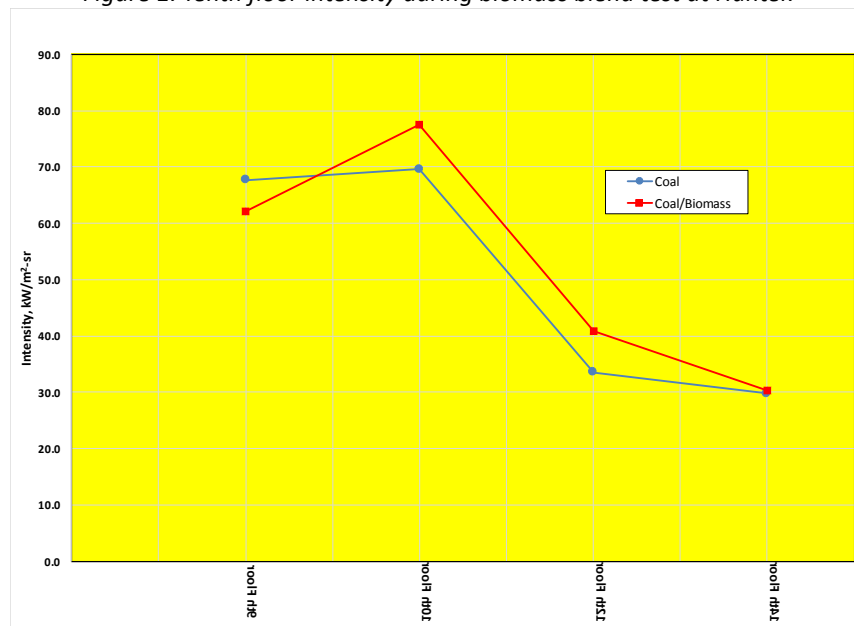*Figure 1. Tenth floor intensity during biomass blend test at Hunter.*

Figure 2. Average intensity comparison between coal and coal-biomass blend.

We refined the radiometer "models" in the Arches code. There are two models, one using orthogonal sweeps with the discrete ordinates model (DO/sweeps) and the other a virtual radiometer (VR) model that uses reverse Monte-Carlo ray tracing. We were concerned by the large discrepancies between the DO/sweeps and VR model results in L1500 simulations and wondered if these differences were bugs or features. We explored the two models in a simplified case, a box with four cold walls (298 K), one hot wall (1800 K), an outlet (298 K), a participating gas, and no particles. Using S10 (128 ordinate directions) for DO model quadrature and a view

angle 5° and 96 rays for the VR model, we compared the computed intensities for three sets of directions (one orthogonal and two non-orthogonal). By running with the finer DO quadrature (and mesh) resolutions, the two models' results differed by <1%. We are finishing up the work with particles and will provide all the information about the analysis in a memo format.

<u>Cooling Plate – Radiative Heat Flux.</u> We also developed an instrument model for measuring the heat flux in the L1500 using data obtained from water-cooled panels. Figure 3(a) shows the panel from the back (flanged) side. Water enters the panel through tube on the far left and exits the panel through the tube on the far right. The inside of the panel consists of baffles as shown in Fig. 3(b). We measured the flow rate of water and the temperatures of the water at the inlet and outlet tubes. Heat flux (q" in W/m^2) to the panel can be determined by Eqn. (1) where $C_{p,H2O}$ is the heat capacity of water, T_{in} and T_{out} are the measured water temperatures, A_{panel} is the area of the panel, and b is a bias correction due to unaccounted for physics in the model.

$$q" = \dot{m}_{H2O} * Cp_{H2O} * \frac{T_{out} - T_{in}}{A_{panel}} + b \qquad (1)$$

The red circle in Figure 3(b) identifies the region where two thermocouples pass through the panel and into the front plate of the panel. These thermocouples are embedded at different depths so that heat flux to the panel can be measured. Thus, the panel itself provides two forms of heat flux measurements.
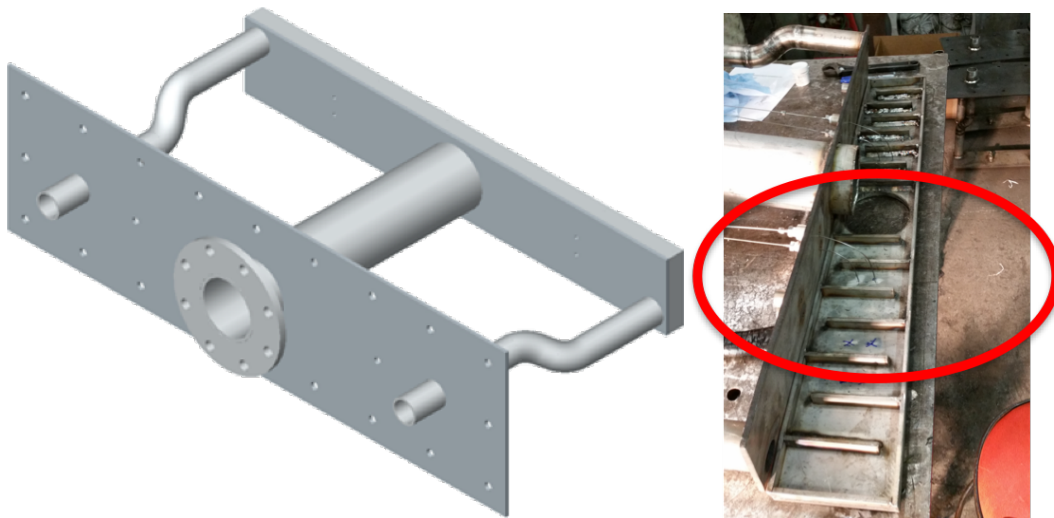

Figure 3. (a) View of water-cooled panel. (b) Two thermocouple pairs are embedded at different depths into the steel face of the panel.

The Bayesian analysis of the instrument model for net heat flux required calibration data for determining model parameters. Unfortunately, we did not calibrate the panel with a source of known heat flux. We only had calibration data for the flow rate of water and uncertainties for the measurements of the inlet and outlet water temperatures. As a result, the bias error in Eqn. (1) is

unknown. To compensate, we performed a Bayesian analysis of the measured heat flux uncertainty using the multi-depth thermocouple data in the front plate as our "experimental" data. We obtained the posterior predictive at each data point; the results are shown in Figures 4 and 5. There were water-cooled panels on the north and south sides of the furnace and the plots represent the measured heat flux at the two panels. The furnace settings on the two days are replicates and the data are plotted relative to the beginning of the time interval. Given the simple instrument model and the many variables that are unaccounted for in the operation of the L1500, the difference in computed net heat flux from November 12 to November 13 is small. There is a large difference in net heat flux between the south (220,000-240,000 W/m² average) and north (150,000-170,000 W/m² average) panels. This difference could be caused by different thicknesses of ash deposits on the panels. The uncertainty is also large due to the lack of true calibration data. More details of this analysis are available in a memo dated 1 August 2019 that is available upon request.
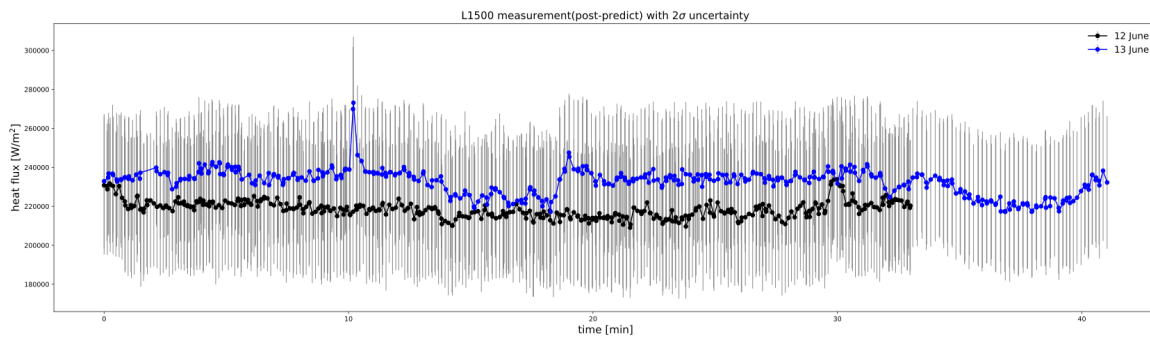

Figure 4. Net heat flux measurements (average with 2σ uncertainty) for the Section 1 South panel during two-time intervals.
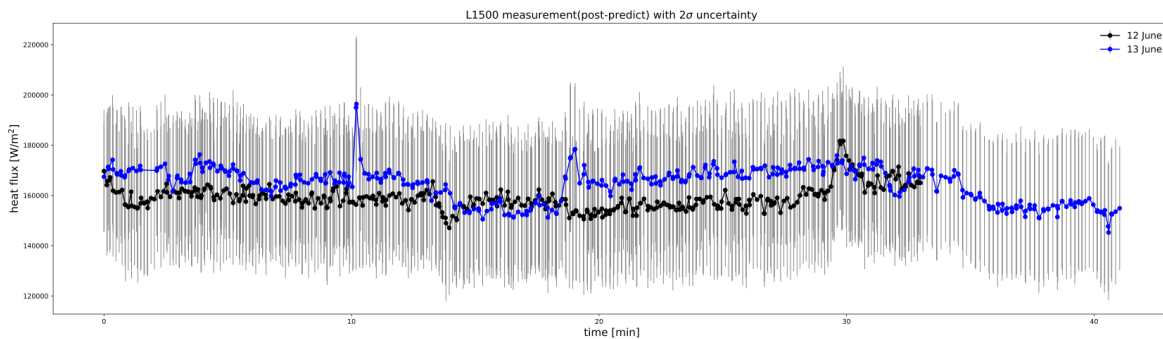

Figure 5.. Net heat flux measurements (average with 2σ uncertainty) for the Section 1 North panel during two-time intervals.

<u>Viscometer and Flame Scanner Instrument Models</u>**.** As part of the data acquisition, the viscosity of the ash deposits is an important parameter in determining the overall heat flux to boiler tubes. While there are several correlations, based on ash composition, which are currently used in the computer simulations, we wanted to obtain our own viscosity data. We located a high-temperature slag viscometer at Principia College that was then donated to the University of Utah. The viscometer needed significant upgrading. With the switch from coal to biomass that occurred during this reporting year, the viscometer was deemed uneconomical to repair because biomass has less than 1% ash and the ash deposits on the boiler walls are minimal. We performed extensive background research for the viscometer instrument model prior to learning that the project would not continue.

With the switch to a biomass-fired boiler in this reporting year, we had new types of measurements that required instrument models. One of those measurements was the strength of the flame as measured by flame scanners. The flame scanners have flexible fiber optic heads with a lens that focuses the incoming radiation into the fibers. At the other end of the fibers is a PbS photocell that is sensitive to infrared radiation. Because these flame scanners are similar in operation to our narrow-angle radiometers, we thought that we could take a similar approach to the instrument model analysis. However, the analysis required that we had access to calibration data or that we could obtain a flame scanner and calibrate it ourselves. After actively pursuing both angles for several months, we were unsuccessful in obtaining calibration data and had to abandon this instrument model.

It is clear that our approach to taking measurements and determining uncertainty needs to be considered from the outset when planning an experiment. The instrument model should be finished prior to the experiment so that it can be properly calibrated and implemented.

Coal Devolatilization

The majority of work done in the final year of coal pyrolysis research for the center was the development of correlations to describe the elemental compositions of primary coal tar and char. The idea is to provide a simple method for improving prediction of the elemental composition of volatiles and char large-scale simulations, thereby improving combustion calculations. An extensive dataset of experimentally measured elemental compositions (CHONS) of coal char and tar at a variety of experimental conditions was used in a cross-validation analysis to test and validate several simple correlations. These elemental composition correlations use several coal and reaction specific variables that are commonly associated with changes in elemental and chemical composition during pyrolysis reactions. A few of the tested model forms used either a measured or a correlated coal aromaticity. Coal aromaticity is measured using ^{13}C NMR spectroscopy, which is expensive and is not a standard test in coal characterization. A small validation analysis was completed to determine the best and most accurate coal aromaticity correlation to use in place of a measured aromaticity value. In all, 44 different model forms were considered for coal aromaticity and 172 were considered for the elemental compositions. These models were evaluated for overall accuracy and best fit as well as minimizing the total number of fitted parameters.

Soot formation

Over the past year, our efforts on soot formation have focused on publication of results, running simulations of the OFC for experimental validation, and developing a library of soot formation models. We have been running simulations of our model in the OFC reactor to compare with experiments performed by Stimpson et al. Results are unexpected, with simulations with soot showing higher temperatures than those without soot. We have spent considerable time investigating the cause of this, whether a model feature, or a bug in the code or problem specification. We expect to publish results of the OFC simulations in 2020 comparing behavior with and without soot, and with different soot models. These will be the first LES of soot formation at pilot-scale of oxy-coal combustion. In addition, we have developed on open-source soot library that includes several soot descriptions, including monodispersed, lognormal, QMOM, MOMIC, and a sectional model. Various chemistry models are included allowing for treatment of gas, coal, and biomass combustion. These models are written in C++, but we are planning Python interfaces.

Differences between biomass and coal in terms of simulation - Atikokan Digital Twin

We are developing the digital twin of a 200 MW, biomass-fired, tower boiler (Atikokan). We are constructing the twin using multi-physics simulations that account the physical processes and a Bayesian methodology to estimate uncertainty in predictions. During this year we completed one complete digital twin cycle and almost completed a second.

The digital twin should be applicable over the range of operating conditions of the actual boiler. For the first digital twin, we wrote scripts to obtain operating conditions and experimental data using two days of collected Atikokan plant data; the boiler produced from 50 to 200 MWN. We also performed analyses on the biomass to obtain the physical properties needed in the simulations. With these analyses and the boiler geometry as inputs, we used Arches to perform the boiler simulations based on a four-parameter design of experiments (DOE). The parameters included two scenario parameters derived from a principle components analysis and two model parameters (burner swirl number and a parameter that affects ash emissivity). We then ran 40 simulations of the Atikokan boiler, each requiring 1098 cores and 72 hours to produce data. We used the digital twin to perform a Bayesian validation and uncertainty analysis. From the analysis, we estimated the uncertainty of the two model parameters and of the quantities of interest (QOIs). Finally, we used the digital twin to predict the heat flux in 20 locations throughout the boiler. As part of this work, we helped write the code for the digital twin algorithm, wrote scripts to automatically create cases for the digital twin and to extract the QOIs, and presented the results of the digital twin at the Western States Section of the Combustion Institute Fall Technical Meeting.

Before proceeding with the second cycle of the construction of the digital twin, we needed to update the Arches simulations to better represent the Atikokan boiler. These updates included fixing the direction of the swirl burners, adding a new inlet for flue gas recirculation, adding a permeable boundary conditions that allows particles to leave the computational domain (this

boundary represents a water surface in the boiler ash hopper), modifying the code so that each particle environment can have a different ash fraction, and removing ash particles that stick to the wall from the simulation, and focusing on the low load (50-150 MWN) operating range. There are four continuous scenario parameters in the DOE (biomass firing rate, secondary air flow rate, air flow rate to burners not firing biomass or tramp air, and the flue glass recycle rate), plus a fifth discrete parameter that represents the two levels of burners being fired under low load (there are five levels total).

There are 20 cases in the DOE for each set of two burners. We then added an additional 20 points to the DOE to see if we could improve the accuracy of the surrogate models for the QOIs. We ran all 40 cases for six sets of two burners (the six most likely to be used together based on plant history). We are in the process of running the remaining three sets of burners with the original 20 DOE points. The total number of cases we will have run for this digital twin is 300. Each case runs on 1134 cores for at least 72 hours on Quartz at LLNL.

VALIDATION/UNCERTAINTY QUANTIFICATION

An advanced V/UQ course had been started in the last few months of the previous reporting year. We continued that effort for the first couple months of this reporting year. Initially the course participation included about a dozen researchers from the center. Topics covered included
* Review of epistemology & philosophy of the scientific method
* Review of probability theory including interpretations of probability & stochastics
* Bayes' law (likelihoods, priors, posterior predictives, nuisance variables, analytical posteriors for canonical problems, gridded solutions for low number of dimensions, sampling methods for higher number of dimensions)
* Gaussian processes for surrogate modeling
* Machine learning (with artificial neural networks) and artificial intelligence
* Decision theory and optimal experimental design
* Bayes graphs, other sources of uncertainty & bias identification
* Student projects

One of the student projects, from the course, extended into the center's primary line of research. Specifically, a radiometer instrument used in the L1500 experiments was fully analyzed using Bayes' law for the instrument calibration and the posterior predictive for measurements in the L1500. The primary advantage was to provided a concrete example of the V/UQ theory to which all the researchers in the center could relate. In addition, the algorithm has been used multiple times since to analyze measurements made by the instrument.

In each year of this program there has been an analysis performed on the BSF (Boiler Simulator Facility at GE/Alstom). Most of these analyses have either used B2B in a low number of dimensions, or they have used a linear approximation for Bayes in a moderate number of dimensions. In this year we have simultaneously performed a moderate dimensional B2B analysis and a full nonlinear Bayesian analysis — using the same dimensions. Having compared the two analysis methods side by side, conclusion are tabulated as follows
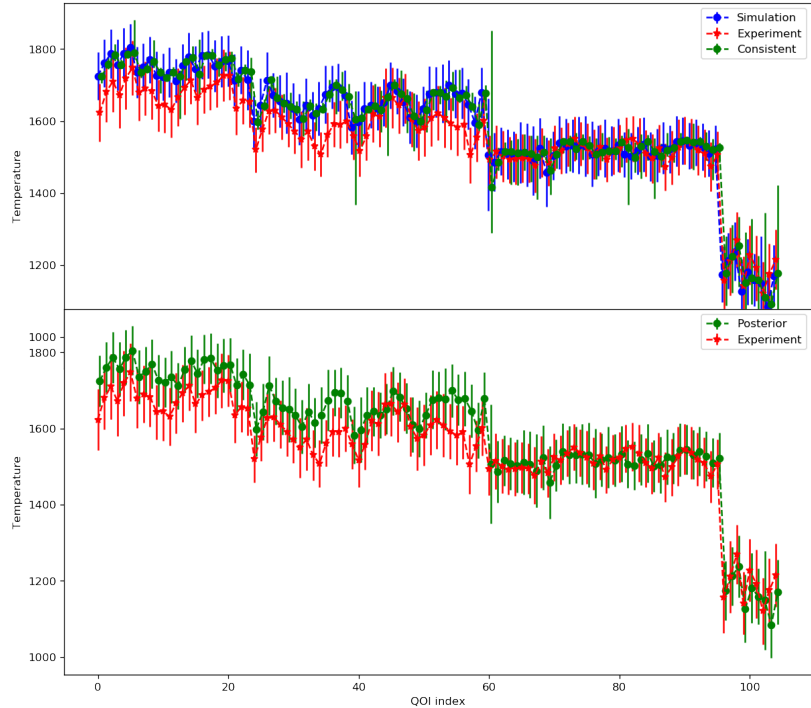

Figure 6. Comparison of UQ methodologies us B2B and Bayes.

B2B / Consistency	Bayes Law
$\alpha_i \leq x_i \leq \beta_i \quad \text{for } i = 1,\ldots,n$ $\ell \leq y_m(x) - y_e \leq u \quad \text{for all experiments } e$	$p(x\,|\,y_e) \propto p(x) \times p(y_e\,|\,x)$
Both combine theory with observations to learn about uncertain parameters & simultaneously evaluate model form.	
Both allow either simultaneous or sequential addition of independent data sets.	
Bounds on x (feasible space)	Distribution over x
ℓ & u must be provided	σ is learned (ideally)
Hard constraint on model form	Soft constraint on model form
L^∞ norm on defect	L^2 norm (most commonly)
Quadratic response easily handled in hundreds of dimensions	Full nonlinear response workable in tens of dimensions.

Through our experience with a couple industry partners, we have recognized that uncertainty itself has less value to the customer than we originally imagined. We feel strongly that there is potential for it to have greater value once we provide the tools to make decisions in the presence of uncertainty. We have been developing experience with Bayesian decision theory. The goal is to provide a digital twin that can reside at a plant, perform calculations in realtime using the

surrogate model and the posterior, make predictions with uncertainty as well as make recommendations which account fo the uncertainty. The LES calculations would definitely be performed offline before hand. The Bayesian inverse could be performed offline as well, or with additional approximations it could be performed online — depending on what the situation called for and what data is available.

Salvatore Iavarone & Gianmarco Aversano both students of Alessandro Parente defended their dissertations in the reporting period. Salvatore has moved on to a postdoc at Cambridge and Gianmarco has joined an engineering-combustion consulting firm.

Coal System V/UQ
Significant improvements were made to the calibration process of the narrow-angle radio-meters. The radiometers output a voltage that is proportional to the intensity incident on upon the thermopile and is also dependent on the temperature of the thermopile itself. Thus, a three-dimensional calibration surface is required. The previous calibration setup - which was in use since August 2018 - blew hot air onto only one side of the radiometer and is referred to as the "Uneven Heating" setup. The calibration improvements were finalized in November 2019 with a new setup that involved a more uniform heating method, the "Uniform Heating" setup

In the initial calibration procedure, data were taken using two multimeters to measure the millivolt signal and thermistor temperature of the radiometer. This method provided point measurements only, so trends as a function of time were not easily observed. As an improvement to the calibration procedure, in August 2019, the radiometers were connected to an Opto-22 system that could simultaneously record the output voltage and thermistor temperature. Figure 7 displays three rows of this opto-recorded, radiometer calibration data. Each row represents radiometer data taken over several minutes while looking at the blackbody set up 600 °C and contains the radiometer's voltage response, the thermistor temperature and the difference in temperature across the radiometer housing.

The first data set (first row) was taken with the "Uneven Heating" setup. The thermistor temperature does not ever stabilize during this time period and the millivolt signal varies from 0.175 to -0.124 mV. This large variation in the millivolt signal throws into question the initial calibration procedure using the two multimeters as it never examined measurement stability as a function of time. The second data set (second row) was also taken with the "Uneven Heating" setup. However, this time, the data was taken after the millivolt signal and thermistor temperature had stabilized at 0.056 mV and 115 °F, respectively. The third data set (third row) also has a stable millivolt signal and thermistor temperature of 115 ° F but this signal is 0.161 mV, a factor of ~3 off from Row 2. Thus, something else was affecting the millivolt signal besides incident intensity and the measured thermistor temperature.

To examine the problem more thoroughly, two thermocouples were placed on the bottom and top of the outer radiometer housing and connected to the Opto system. These plots are seen in

the third column in Figure 7 With these data, it was discovered that the voltage signal is also dependent on the temperature profile throughout the thermopile, not just the measured thermopile temperature. The first data set in which not even the thermistor temperature is stable shows an extreme difference in temperature between the top and bottom the radiometer (~65 °F). The stable 0.056 mV signal in the second row is a fairly rare occurrence in which there is a significant but stable temperature gradient across the radiometer due to the "Uneven Heating" setup. The third row contains data from the "Uniform Heating" set and has a very small temperature gradient across the radiometer (~1.3 °F) and thus should yield the desired voltage output.
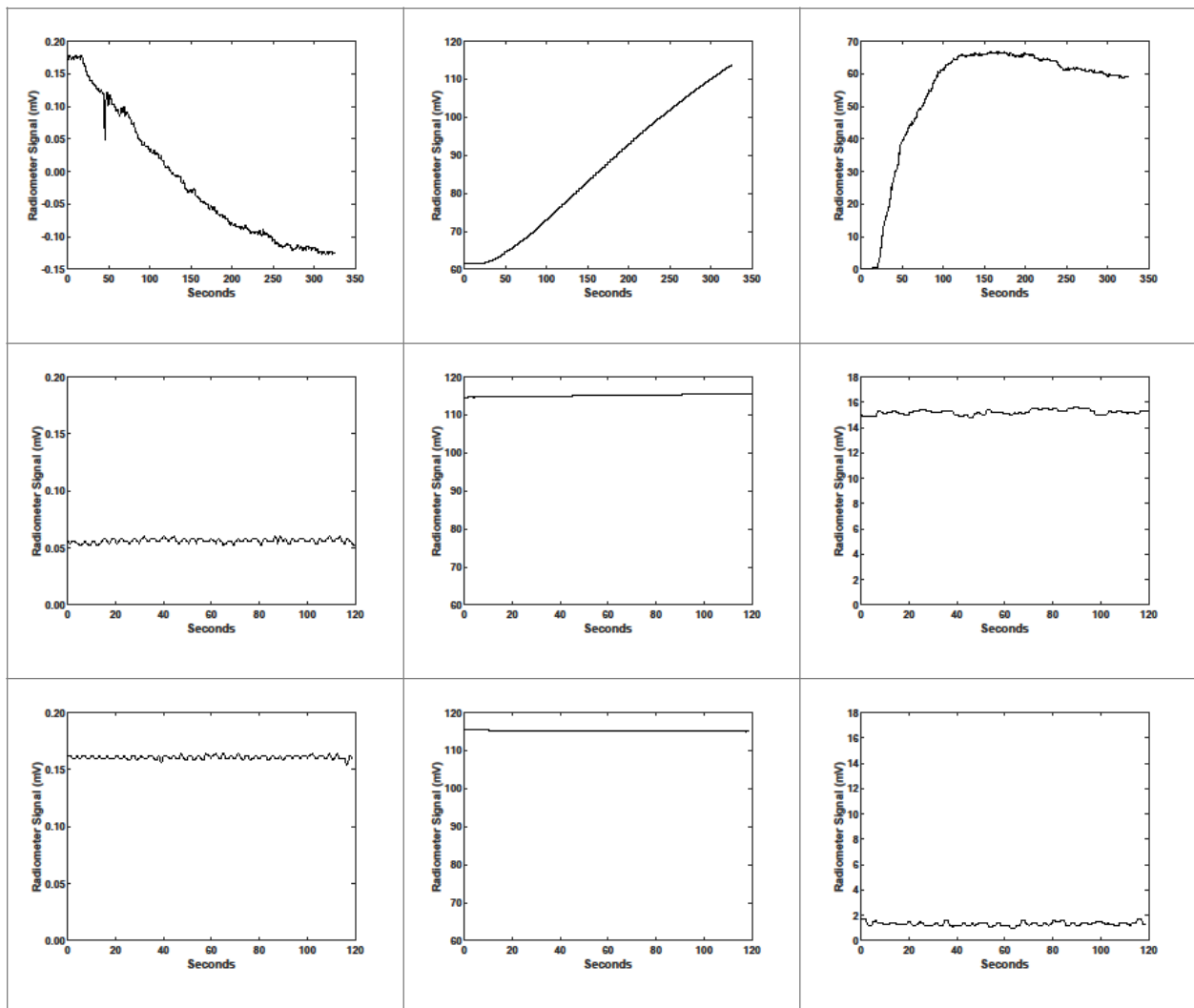

Figure 7. Three sets of radiometer calibration data. Each set contains the radiometer's voltage response, the thermistor temperature and the temperature gradient across the radiometer housing.

Thus, we would expect data taken with the initial calibration setup but with Opto to check for stability should provide mostly repeatable data but could occasionally provide outliers. With the improved calibration setup, the use of Opto and thermocouples to minimize the temperature gradient across the radiometer, we would expect very repeatable data.

The calibration data points taken at a blackbody temperature of 600 °C are shown for the different calibration setups in Figure 8. When the "Uneven Heating" setup was used in conjunction with the multimeter, there is a large variation. The same setup when using Opto to check for measurement stability results in a much tighter cluster but with a few outliers. The "Uniform Heating" setup with Opto produced the most repeatable calibration data.
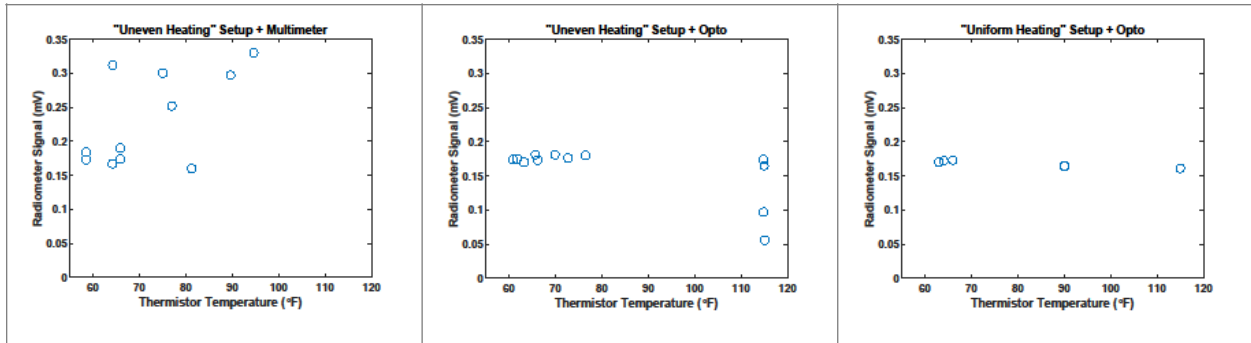

Figure 8. Calibration points taken at a blackbody temperature of 600 °C for each calibration iteration. The data is plotted with measured thermistor temperature versus radiometer signal.

As discussed in the Physics section, a physics-based instrument model and Bayesian analysis was performed to convert the measured voltage and thermistor temperature into an intensity distribution. Figure 9 shows the calculated intensity over a 45-minute interval in the L1500 measured by a radiometer in the near-burner region using first the calibration data from the "Uneven Heating" and then with the data with the "Uniform Heating" setup and Opto-22. The dotted lines represent the 95% confidence interval of the intensity. The average intensity value does not change much between calibrations but the change in the confidence interval is significant. The confidence interval reduces by a factor of 4.3 when using the new calibration setup.

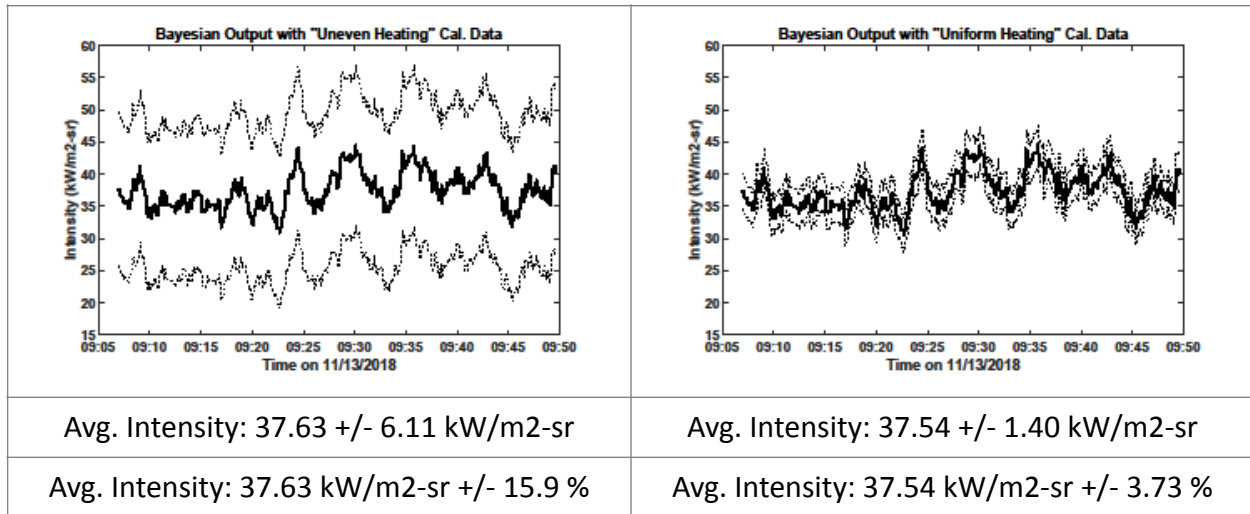| Avg. Intensity: 37.63 +/- 6.11 kW/m2-sr	Avg. Intensity: 37.54 +/- 1.40 kW/m2-sr
Avg. Intensity: 37.63 kW/m2-sr +/- 15.9 %	Avg. Intensity: 37.54 kW/m2-sr +/- 3.73 %

Figure 9. Smoothed (20-point rolling average) posterior predictive intensity and associated 95% confidence interval calculated by Bayesian analysis using calibration data from Left) the old setup and multimeters and Right) the new setup and Opto. These data points were taken in the L1500 furnace 2 feet downstream from the burner.

Atikokan Boiler Plant

This year, our major focus shifted from coal to biomass. Analyses were shifted to the Atikokan Ontario biomass facility. The change has revealed a need for a broader analysis to include parameters that previously were not addressed. Part of the efforts of the VUQ team is to provide support to the development of the digital twin for the Atikokan plant. One of the essential components of the predictive capabilities of the digital twin methodology, is the development of surrogate models. We have refined the surrogate modeling methodology with Gaussian Processes to provide accurate representations of the simulation space and streamline the Bayesian Analysis upon which the digital twin methodology relies. The surrogate models we have provided, correspond to the prediction of 20 heat flux locations throughout the boiler, oxygen and NOx concentration at the outlet, several temperature measurements throughout the boiler, and the equivalent power generated by the heat transfer surfaces. The surrogates are also generated for each firing mode the boiler is operating at, and are determined by pairs of levels simultaneously firing biomass. The total number of firing modes we have been able to represent are 8 and their combinations levels (L) are: L(1-2), L(1-3), L(1-4), L(1-5), L(2-3), L(2-4), L(3-4), L(4-5). They can be read as level one and two, L(1-2) for instance.

Sensitivity Analysis The sensitivity analysis includes many more parameters than in previous cycles. Table 1 includes all the parameters that have been considered, and the ones with their respective case ID have been analyzed first, due to their potential impact for the biomass cases.

Figure 10 shows the results of the Sobol sensitivity analysis done on the parameters. The analysis included main and total effects. Because the comparison between main and total effects was similar we can say that secondary or pair-wise interaction between parameters is minimal. This comparison for a particular QOI is presented in Figure 11.

Table 1. Sensitivity to model parameters.

Parameters (H)		Case ID	Nominal Value	Uncertainty	Up Corner	Down Corner
abs_Coef			0.636053693	0.24806094	0.884114633	0.387992753
PC1_O2			-1.83158207	-0.714317007	-2.545899078	-1.11726506
PC2_O2			1.089131019	0.424761097	1.513892116	0.664369922
Ae O2		Case 1	2.021644437		0.590395073	6.92256155
Ea O2		Case 2	11202.51147		7588.908543	14816.1144
PC1_CO2			2.00337885	0.781317751	2.784696601	1.222061098
PC2_CO2			-0.183367821	-0.07151345	-0.254881271	-0.11185437
Ae CO2		Case 3	2054.992846		2666.597056	1583.664689
Ea CO2		Case 4	63805.90996		69935.02124	57676.79868
ksi		Case 5	0.97266	0.3793374	1.3519974	0.5933226
Relaxation coeff		Case 6	0.005		0.05	0.001
k_ash_sigma		Case 7		-0.277707214	-0.277707214	-0.27770721
T_hardened		Case 20	1950.06337	380.2623572	2330.325727	1569.801013
v_hit		Case 8	0.6202	0.241878	0.862078	0.378322
T_devol	T_mu	Case 9	832	216.32	1048.32	615.68
T_devol	T_sig	Case 10	134.6493799		189.4000451	79.89871477
SgO		Case 11	1010.8	394.212	1405.012	616.588
porosity		Case 12	0.6		0.7	0.35
ash fluid temperature	T_hemi	Case 33				
ash fluid temperature	T_soft					
ash fluid temperature	T_fluid	Case 21	1510	196.3	1706.3	1313.7
viscosity pre-exp. factor			1.40E-15		1.78164E-18	1.10519E-12
ln(viscosity pre-exp)		Case 13	-3.42E+01	-6.67E+00	-4.09E+01	-2.75E+01
viscosity activation energy		Case 14	49.42441876	9.637761657	59.06218041	39.7866571
HHV			20952.63	4085.76285	25038.39285	16866.86715
particle density		Case 16	1300	253.5	1553.5	1046.5
particle initial void fraction		Case 17	0.1		0.35	0.08
Composition			ND lignite		German Lignite	
Ta		Case 22	19910.00	7764.90	27674.90	12145.10
A		Case 23	2.29087E+11		3.76011E+13	1395725458
ln(A)			26.15736666	5.100686498	31.25805315	21.05668016

|						
soot density			1900	370.5	2270.5	1529.5
particle thermal cond.		Case 24	4	1.56	5.56	2.44
K_main		Case 18	3.45	0.897	4.347	2.553
enamel thickness (mm)		Case 19	3.09E-02		1.5	0.5
t_scale dep (s)			788836.091		432000	129600
Wall emissivity			0.8	0.104	0.904	0.696
Rad solve frequency			20		40	10
Angular Discretization			8		16	4
Re_limit			10000	3900	13900	6100
Gas phase temporal scheme			2nd order		3rd order	
opl			0.9488	0.37	1.32	0.58
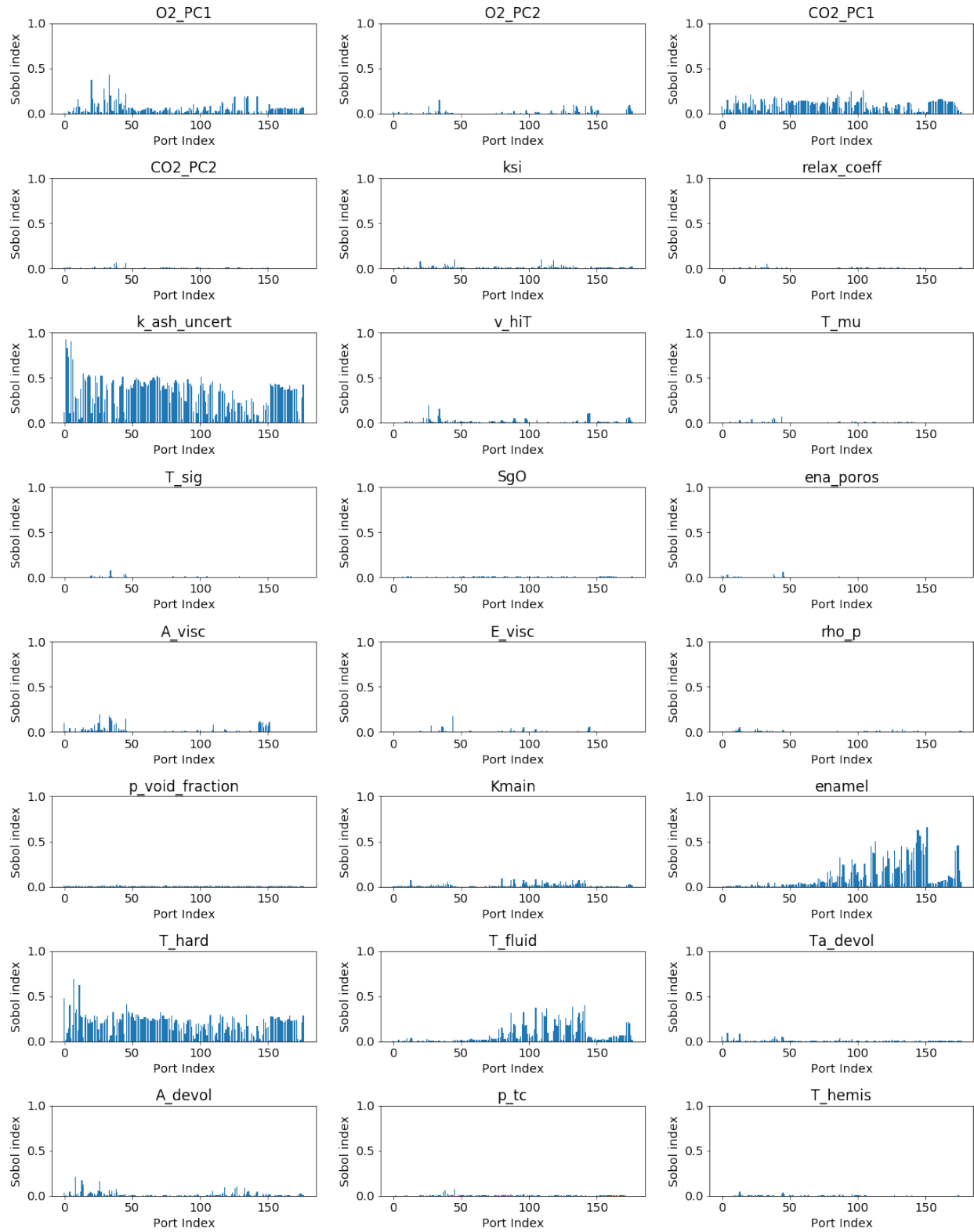
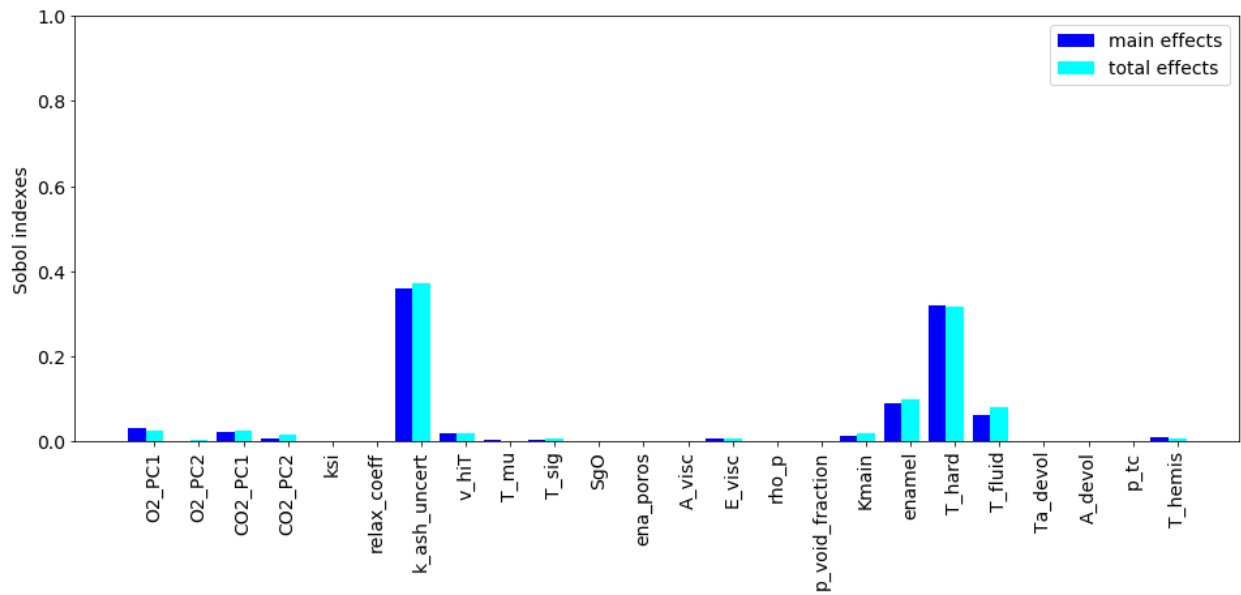**Figure 10.** *Sobol sensitivity for the ID cases in Table 1.*

Figure 11. *Comparison between total and main effects in the Sobol sensitivity analysis.*

<u>Uncertainty Quantification</u>. The Sobol sensitivity analysis yields the 6 most sensitive parameters in our modeling approach for the BSF. Twenty-one (21) simulations were ran for these parameters, whose values were chosen from a Latin-hypercube design. Table 2 shows the values of the parameters for each case

Table 2. Parameter design for the most sensitive model parameters in the BSF

	$PC1_{O2}$	$PC1_{CO2}$	σK	δ_{enam}	T_h	T_{fluid}
μ	-2.4	1.4	-0.39	0.7521	2117.5	1608
σ	0.12	0.3333	0.004033	0.1865	15052.1	3201.3
Case 1	-2.65	1.02	-0.45	0.36	2207.81	1625.15
Case 2	-2.62	0.72	-0.40	0.77	2144.06	1664.35
Case 3	-2.71	0.57	-0.42	1.11	2314.06	1654.55
Case 4	-2.57	0.47	-0.34	0.06	2048.44	1512.45
Case 5	-2.95	2.03	-0.49	1.26	2282.19	1600.65
Case 6	-2.68	1.83	-0.29	0.40	1910.31	1571.25
Case 7	-2.35	1.98	-0.35	1.29	2154.69	1620.25
Case 8	-1.99	2.13	-0.32	0.58	2165.31	1517.35
Case 9	-2.47	1.88	-0.32	0.66	1963.44	1674.15
Case 10	-2.38	1.43	-0.33	0.47	2112.19	1551.65

	$PC1_{O2}$	$PC1_{CO2}$	σ_K	δ_{enam}	T_h	T_{fluid}
Case 11	-2.86	1.52	-0.40	1.14	1995.31	1698.65
Case 12	-2.41	2.23	-0.50	0.62	2101.56	1595.75
Case 13	-2.77	0.82	-0.31	0.88	2005.94	1634.95
Case 14	-2.20	2.07	-0.48	0.14	2027.19	1532.05
Case 15	-2.08	1.37	-0.48	1.41	1952.81	1679.05
Case 16	-2.99	1.92	-0.34	0.10	1931.56	1536.95
Case 17	-1.84	0.88	-0.49	0.02	2250.31	1522.25
Case 18	-2.50	0.63	-0.37	0.70	2271.56	1649.65
Case 19	-1.90	2.18	-0.33	0.73	2292.81	1605.55
Case 20	-2.02	2.33	-0.45	0.28	2037.81	1639.85
Case 21	-2.26	1.27	-0.41	0.92	2303.44	1546.75

Based on the 21 simulations, surrogate models for each QOI in the boiler were constructed using Gaussian Process regression. Figure 13 shows parity plots for selected surrogates. Makov-chain Monte Carlo sampling implemented in the emcee open-source library (*https:// emcee.readthedocs.io/en/stable/*) was used with the surrogates in order to sample the 9-dimensional space produced by the distribution of the values of the model parameters and the total uncertainty associated to the QOI's of the system. Figure 13 shows corner plots with slices of this distribution.
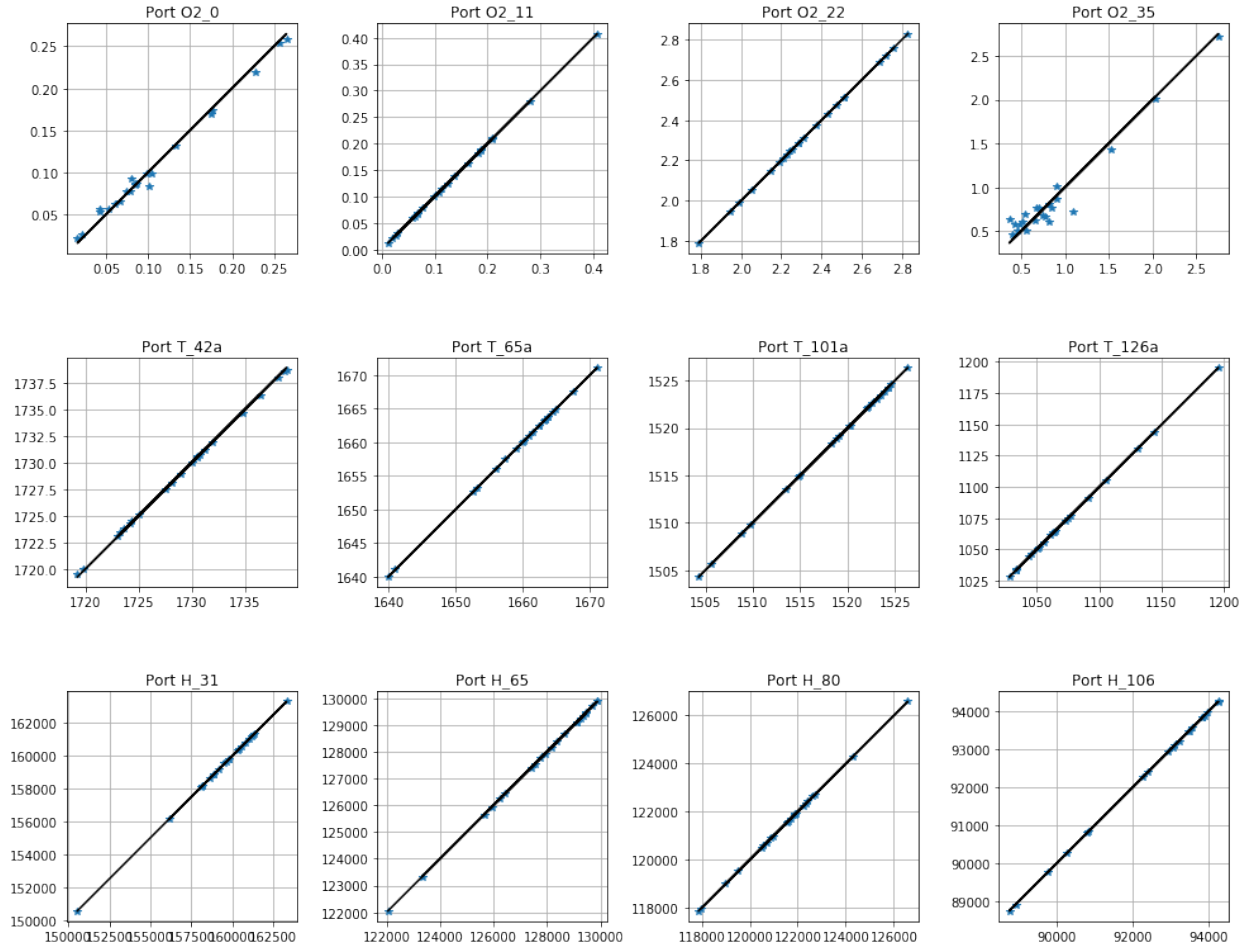
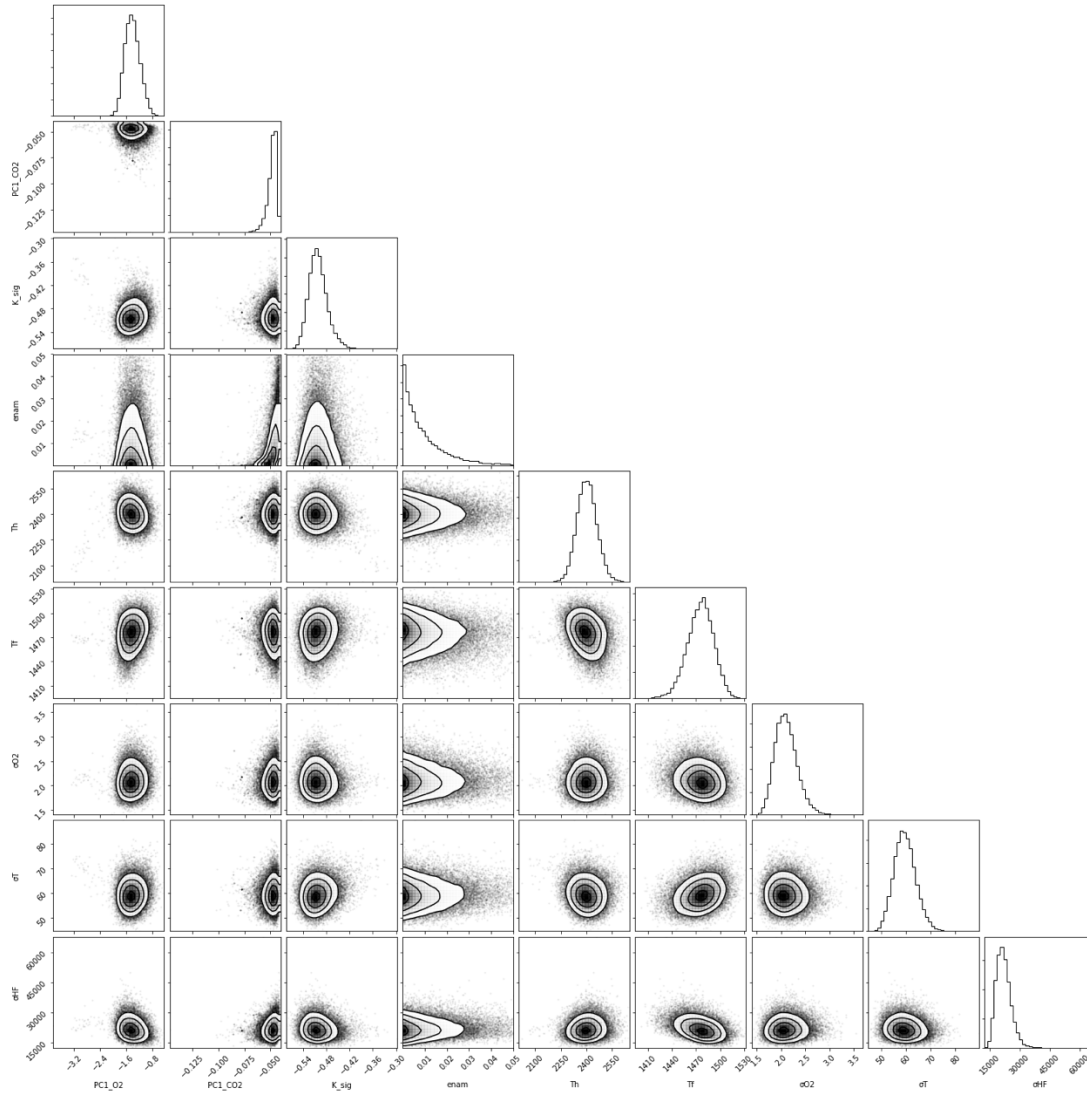**Figure 12.** *Prediction of surrogate models using the simulation data.*

Figure 13. *Distribution of uncertain model parameters and QOI's*

This multidimensional distribution was used to estimate the posterior prediction of the QOI's of the system, as presented in Figure 14.
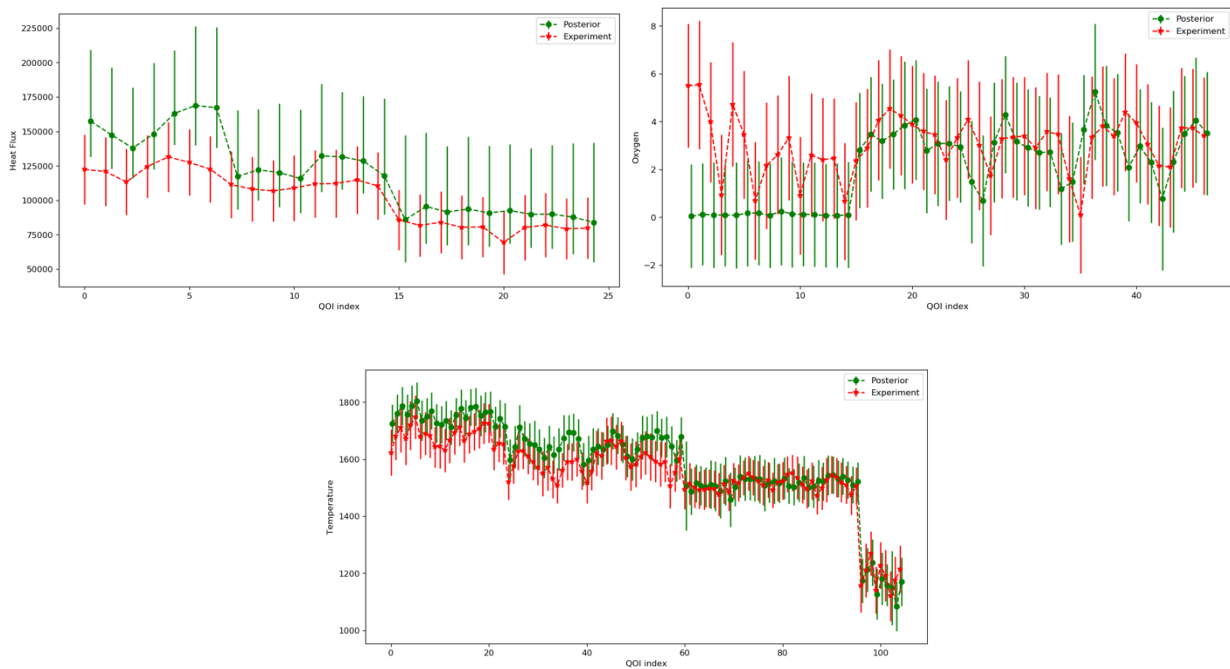

Figure 14. Posterior prediction for the 3 QOI's of the BSF: Heat Flux, Oxygen concentration and Temperature.
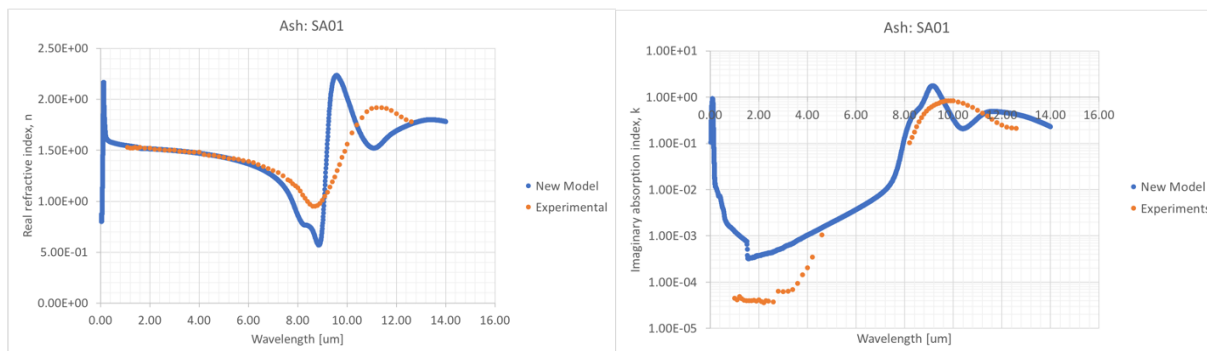

Figure 15: Comparison against experimental data for n and k from a synthetic ash with the following compositions. SiO_2: 59.40%, Al_2O_3: 28.49%, CaO: 11.28%, Fe_2O_3: 0.82%

Spectral properties of Ashes The shift from coal to biomass made it necessary to reformulate the way we compute the spectral properties of the fuel mineral content. Usually, the mineral content of biomass ashes is rich in the alkali oxides: CaO, MgO, Na_2O, K_2O, which are marginally present in coal ashes. The influence of these oxides was not accounted for in previous cycles of the emissivity model calculation, but their influence could be important whenever their presence is substantial in the biomass fuel. The index of refraction is computed now from the effective dielectric function of the composite matrix of mineral content as an effective average of the

oxides' dielectric functions[1]. The Bruggeman's model was chosen to compute the effective dielectric function of the slag composite from which effective complex indexes of refraction will be obtained. Figure 15 shows the comparison against experimental data for the synthetic ash SA01 reported in J. L. Ebert's publication[2].

Model discrepancy in B2BDC.

One of the main accomplishments of Year 6 is the incorporation of model discrepancy into the Bound-to-bound data collaboration (B2BDC) framework in order to resolve dataset inconsistency and perform prediction. The addition of this discrepancy term is well motivated when the inconsistency is believed due to an inadequate model rather than mis-specified experimental bounds. In our framework, the discrepancy is formulated as a linear combination of basic functions depending only on the scenario parameters. This structure leads to an extended feasible set in the space defined by the uncertain model parameters and discrepancy coefficients.

B2BDC, waves, and ellipsoids.

We have continued our work in investigating similarities between techniques such as Bayesian history matching and B2BDC. In particular, we adopt the formalism of history matching's "waves" to iteratively assemble datasets in B2BDC. This strategy prioritizes accurate representation of QOIs in that only QOIs that can be accurately fit with B2BDC surrogates (quadratic/polynomial and rational quadratic models) are included during each iteration. As the iterations progress, QOIs are fit over the current stage's feasible set. Those that have accurate surrogate models are then incorporated into the dataset (with the corresponding experimental data) as model-data constraints, thus reducing the feasible region for the next iteration. Another addition is the inclusion of minimum volume ellipsoids as a way of incorporating sample-based feasibility criteria into B2BDC.

Uniform sampling to the feasible set.

We have continued our work on developing sampling strategies for B2BDC feasible sets. The current work focuses on comparing the impact of different assumptions -- specifically, Gaussian versus uniform likelihood – on the results of a UQ analysis. A key component of this research is the investigation of two common sampling strategies, the hit-and-run sampler and Gibbs sampling, for generating uniforms samples from a feasible set. Recall that in B2BDC, the feasible set is generally a collection of nonconvex quadratic inequalities. A manuscript detailing this research is currently in preparation.

---

[1] Bohren, C. F. & Huffman, D. R., 2008. Absorption and Scattering of Light by Small Particles. s.l.:Wiley Science Series; John Wiley & Sons

[2] Ebert, J. L., 1994. Infrared Optical properties of Coal Slag at High Temperatures., s.l.: Stanford University

PUBLICATIONS & PRESENTATIONS

A. Sanderson, A. Humphrey, J. Schmidt, R. Sisneros, and M. Papka. *In situ visualization of performance metrics in multiple domains.* Workshop on Programming and Performance Visualization Tools (ProTools19), Nov 2019.

O. Díaz-Ibarra, J. C. Parra-Alvarez, S. Harding, L. Marshall, S. Smith, J. Thornock, M. Hradisky, J. Spinti, and P. Smith. *Development of a digital twin for a biomass boiler: Preliminary results.* 2019 WSSCI Fall Technical Meeting, Albuquerque, NM, October 14-15, 2019.

J. C. Parra-Alvarez, O. Díaz-Ibarra, S. Smith, M. Zhou, B. Isaac, and P. Smith. *Modeling the effect of ash build-up in fire-side furnace on radiation heat transfer.* 2019 WSSCI Fall Technical Meeting, Albuquerque, NM, October 14-15, 2019.

O. Díaz-Ibarra, J. Thornock, S. Smith, B. Isaac, D. Harris, D. Chen, Z. Li, and P. Smith. *Bayesian Parameter estimation for a large-eddy simulation (LES) based coal NOx model*. 11th U.S. National Combustion Meeting, Pasadena, CA, March 24-27, 2019.

T. Draper, K. Scheib, S. Harding, M. Hradisky, J. Spinti, T. Ring, A. Fry, M. Backman, A. Gunnarsson, K. Andersson, and E.G. Eddings. *A comparison of heat transfer measurements between pulverized-coal and 85% coal/15% biomass co-firing combustion in a 1.5 MW pilot-scale furnace*. 44th International Technical Conference on Clean Energy, Clearwater, FL, June 16-21, 2019.

A. Fry, S. Fakourian, K. Andersson, T. Allguren, A. Gunnarson, J. Wendt, Y. Wang, X. Li, M. Backman and E.G. Eddings. *Comparison of Combustion Performance and Fouling Behavior While Firing a 15wt% Blend of Prepared Woody Biomass with Coal and Pure Coal in a 1.5 MW Pilot-scale Furnace*. 44th International Technical Conference on Clean Energy, Clearwater, FL, June 16-20, 2019.

Richards, A.P., C. Johnson, and T.H. Fletcher, *Correlations of the Elemental Compositions of Primary Coal Tar and Char.* Energy & Fuels, 2019. **33**(10): p. 9520-9537.

H. Shen (申浩树), Y. Wu (吴玉新), M. Zhou (周敏敏), S.T. Smith, H. Zhang, G. Yue, *"Identification of the initial particle size distribution for coal combustion simulations,"* AIChE Journal, 2019, vol. 65, issue 8, p. e16610,

J.C. Parra-Alvarez, B.J. Isaac, M. Zhou (周敏敏), S.T. Smith, T. Ring, S. Harding, P.J. Smith, *"Radiative Properties of Coal Ash Deposits with Sintering Effects,"* Energy & Fuels, 2019, vol. 33, issue 7, pp. 5903-5910, .

Z. Zhang (张志), Y. Wu (吴玉新), D. Chen (陈登高), H. Shen (申浩树), Z. Li, N. Cai, M. Zhou (周敏敏), S.T. Smith, J.N. Thornock, B.J. Isaac, *"A semi-empirical NOx model for LES in pulverized coal air-staged combustion,"* Fuel, 2019, vol. 241, pp. 402-409, DOI: .